PAPER

Check for updates

Triboelectric nanogenerator for harvesting ultra-high-speed wind energy with high-frequency output†

Yanan Bai,[ab] Wenxuan Zhu,[ab] Maoyi Zhang,[a] Md Al Mahadi Hasan, [ad] Chris R. Bowen [c] and Ya Yang [*abd]

As a leading and potential renewable energy alternative, harvesting wind energy has become an essential solution to global energy challenges. However, wind turbines face challenges in harvesting wind energy due to their relatively high cost and limitations associated with the operating wind speed. To overcome these challenges, we propose a fluttering wind-driven triboelectric nanogenerator, mainly achieved by changing the vibration triboelectric layer. Conclusively, wind flow can be converted into electric power at airflow speeds up to 81 m s^{-1} at a significantly low cost. A higher-frequency signal output was realized for the same wind speed, eventually reaching the frequency of 12 260 Hz. At the same time, we achieved more than 3000 V voltage output by changing the size of the fabricated device. This work provides a pioneering strategy for harvesting energy across a broad range of wind speeds, showcasing the advantages of effective wind energy collection at extremely high speeds producing ultra-high output frequency; addressing their advantages over conventional wind energy harvesting technologies.

1. Introduction

As a result of global warming and the scarcity of fossil fuels, it is crucial to search for low-cost and renewable clean energy sources to convert renewable forms of energy into electrical energy.[1–4] Wind power generation is a particularly promising form of renewable energy. Due to its large energy capacity and cost-effectiveness, it has gradually attracted the attention of researchers.[5–8] However, at present, the utilization of wind energy on the earth is not sufficient, especially the high-altitude ultra-high-speed wind energy is still lacking in collection and utilization. This part of energy accounts for a large proportion of wind energy, so it is necessary to collect such ultra-high wind-speed energy.[9] Typically, wind turbines are the primary devices for converting wind flow into electricity. However, the structure of wind turbines limits their scope of application.[10–13] Most importantly, due to the limitations of the operational

rated speeds, conventional electromagnetic generators continue to face challenges in collecting wind energy at ultra-high speeds. The operating wind speed of traditional wind turbines is usually lower than 30 m s^{-1}. When the wind speed exceeds this threshold, the blades and supporting structures are subjected to increased mechanical stress, which may lead to deformation and even damage of the wind turbines, causing serious safety hazards and reducing energy conversion efficiency. The triboelectric nanogenerator (TENG) is a new type of energy harvesting technology for collecting high-entropy energy. It can effectively convert wind energy into electrical energy and thus has received extensive attention.[14–16]

In recent years, TENG has been widely used for wind energy harvesting. Its advantages include cost-effectiveness, high output voltage, material flexibility, and a simple manufacturing process.[17–19] Additionally, TENGs do not generate strong magnetic fields and produce minimal noise during operation. Thanks to their flexible and scalable structural design, TENGs can be easily integrated with infrastructure such as buildings without causing adverse effects on living organisms or the environment. In terms of device structure, TENGs designed for wind energy harvesting can generally be divided into two categories: namely, rotating structures[20–22] and fluttering structures.[8,12,23,24] Due to the limitation of the structure, the rotating TENG will lose part of the energy in the form of heat, and it is easily damaged under high-speed conditions and is difficult to use widely.[15] In contrast, TENG based on flutter/vibration structure can reduce energy loss and collect wind energy under breeze/ultra-high speed. In addition, the TENG based on

aBeijing Key Laboratory of Micro-Nano Energy and Sensor, Center for High-Entropy Energy and Systems, Beijing Institute of Nanoenergy and Nanosystems, Chinese Academy of Sciences, Beijing 101400, P. R. China. E-mail: yayang@binn.cas.cn

bCenter on Nanoenergy Research, Institute of Science and Technology for Carbon Peak & Neutrality, Key Laboratory of Blue Energy and Systems Integration (Guangxi University), Education Department of Guangxi Zhuang Autonomous Region, School of Physical Science & Technology, Guangxi University, Nanning 530004, China

cDepartment of Mechanical Engineering, University of Bath, BA27AK, UK

dSchool of Nanoscience and Engineering, University of Chinese Academy of Sciences, Beijing 100049, P. R. China

† Electronic supplementary information (ESI) available. See DOI: https://doi.org/10.1039/d5ta00649j

This journal is © The Royal Society of Chemistry 2025

J. Mater. Chem. A, 2025, **13**, 9101–9110 | **9101**

the flutter structure is easier to integrate into the array and provides higher output frequency.[25] Currently, there is relatively few research studies on wind energy collection under ultra-high speeds. In this regard, the majority of research to date has primarily focused on wind energy collection at speeds below 35 m s^{-1}. In comparison, it is necessary to address extreme speeds (>35 m s^{-1}) to improve the overall performance of TENGs. In our research, TENG is used to collect wind energy under the condition of speed exceeding 81 m s^{-1}, and the ultra-frequency signal (12 260 Hz) is realized, which provides an effective way to realize the conversion of ultra-high-speed wind energy into electric energy.

Here, we report on a novel double-ended fixed fluttering structure triboelectric nanogenerator that can collect wind energy and convert it into electrical energy with a high voltage output at extreme speeds exceeding 81 m s^{-1}. Furthermore, our research demonstrated that the wind-driven TENG produces high-frequency signals, with the highest output signal frequency reaching 12 260 Hz, and the time interval between two signal peaks is at least 70 μs. This represents a significant improvement compared to conventional electromagnetic generators and previously reported technologies in the literature. We have also designed a double-ended TENG with an effective vibration length of 1 m, which can produce an output voltage exceeding 3000 V to address a wider range of applications in urban settings, such as collecting wind energy generated by urban rail subways and high-speed trains.

2. Results and discussion

2.1. TENG principle and comparison

In Fig. 1a, a physical representation of a commercially available conventional micro three-phase alternating current electromagnetic generator (EMG) is shown, along with an explanation of its working principle. The first step in the working principle is to capture the kinetic energy from wind flow in the natural environment through a wind turbine. This kinetic energy is then converted into rotational mechanical energy, which drives the rotation of an electromagnetic generator. By using electromagnetic induction, the rotational mechanical energy is
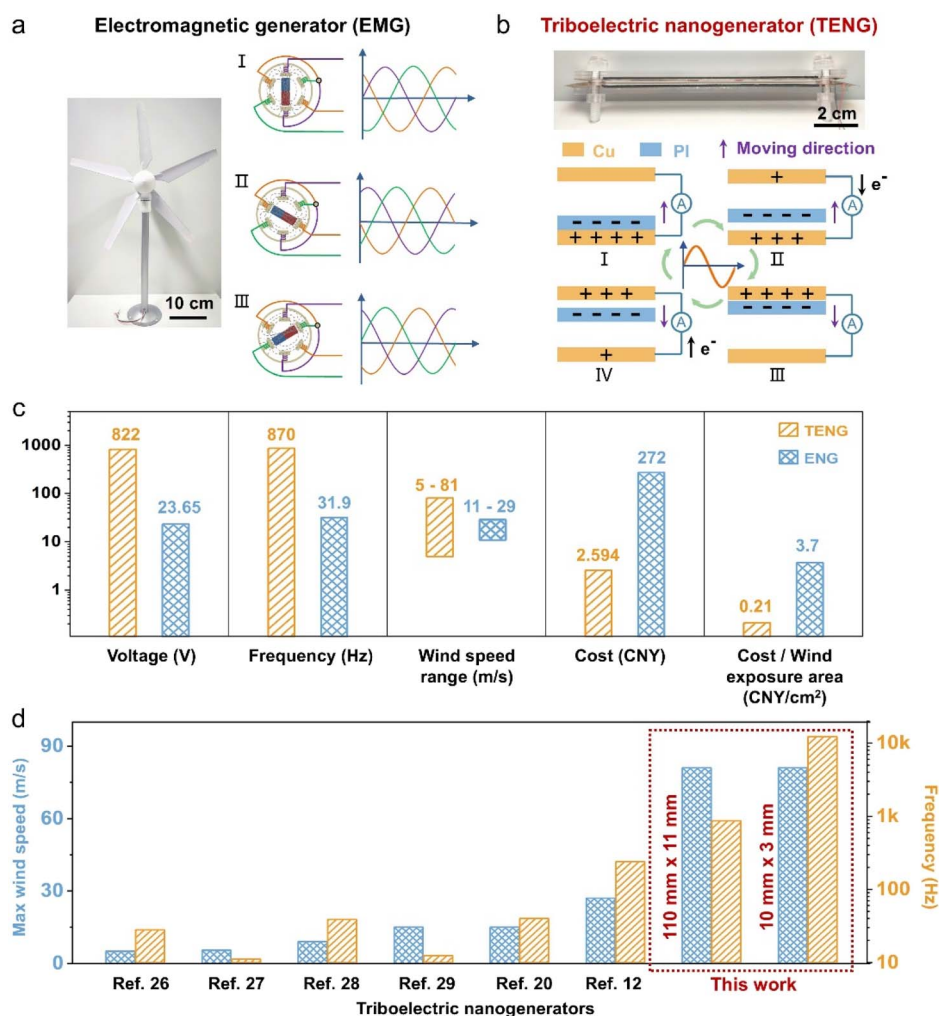

Fig. 1 TENG principle and comparison. (a) Image and working schematic of commercial EMG. (b) Image and working schematic of the developed TENG. (c) Comparison of the correlation coefficients between EMG and TENG. (d) Measured maximum with-stand wind speed and frequency, which are compared with recent studies.

9102 | J. Mater. Chem. A, 2025, **13**, 9101–9110

This journal is © The Royal Society of Chemistry 2025

transformed into electrical energy. The principle behind the generator involves using a rotating magnet and three sets of fixed coils that intersect the rotating magnetic flux lines, thereby generating three-phase asynchronous currents, as shown in the lower part of Fig. 1a. Fig. 1b (upper part) illustrates the TENG specifically designed for wind energy harvesting. It employs a dual-ended fixed structure, with acrylic plates serving as the stationary support and copper foils acting as both upper and lower electrodes. Additionally, a polyimide (PI) film is used as the vibrating layer to generate signals through friction with the electrodes. The reader can refer to Fig. S1† for a schematic representation of the device structure. The lower part of Fig. 1b illustrates the working principle of TENG. The working principle of this device is to capture the kinetic energy of the wind, resulting in the intermediate friction layer vibrating and coming into contact with the friction materials on the upper and lower surfaces. Through frictional electrification and electrostatic induction, the TENG generates an internal potential difference that leads to a flow of charge between the top and bottom electrode, thereby converting wind energy into electrical energy. When there is no wind, the PI film does not vibrate, so no charge transfer occurs, and no electrical signal is generated. When the wind blows, the PI film flutters upward and downward; when it vibrates upward due to electrostatic induction, the charge is gradually transferred to the Cu electrode on the

bottom surface, and the electron flow is shown in the diagram. When the PI film vibrates downward, charges gradually transfer to the upper surface of the Cu electrode in the direction shown in Fig. 1b. This process repeats as the PI film flutters in an airflow. In Fig. 1c, the parameters of the TENG with an effective vibration size of 110 mm × 11 mm are compared with those of a commercial wind-driven micro-EMG. This demonstrates that the TENG can achieve higher voltage and higher signal output frequency, withstand higher speed at lower cost, and have a lower cost per square centimeter of wind-facing area. These highlighted advantages of our TENG compared to the EMG underscore the significance and potential importance of the new device structure. Table S1† outlines the estimation of TENG costs and the unit prices of components. In recent years, there has been extensive research on TENG for collecting low-speed wind (breeze), but there has been little research on understanding the operation of a TENG at ultra-high speeds (>35 m s^{-1}). Here, the TENG was capable of operating at 81 m s^{-1}, and a reduction in the device size enabled us to achieve a TENG with a higher frequency output signal at the same speed. The signal frequency can be as high as 12 260 Hz for a TENG with device dimensions of 10 mm × 3 mm. A comparison of the maximum speed affordable and the maximum frequency achievable, as reported in previous literature, is shown in Fig. 1d.[12,20,26–29] This also highlights that
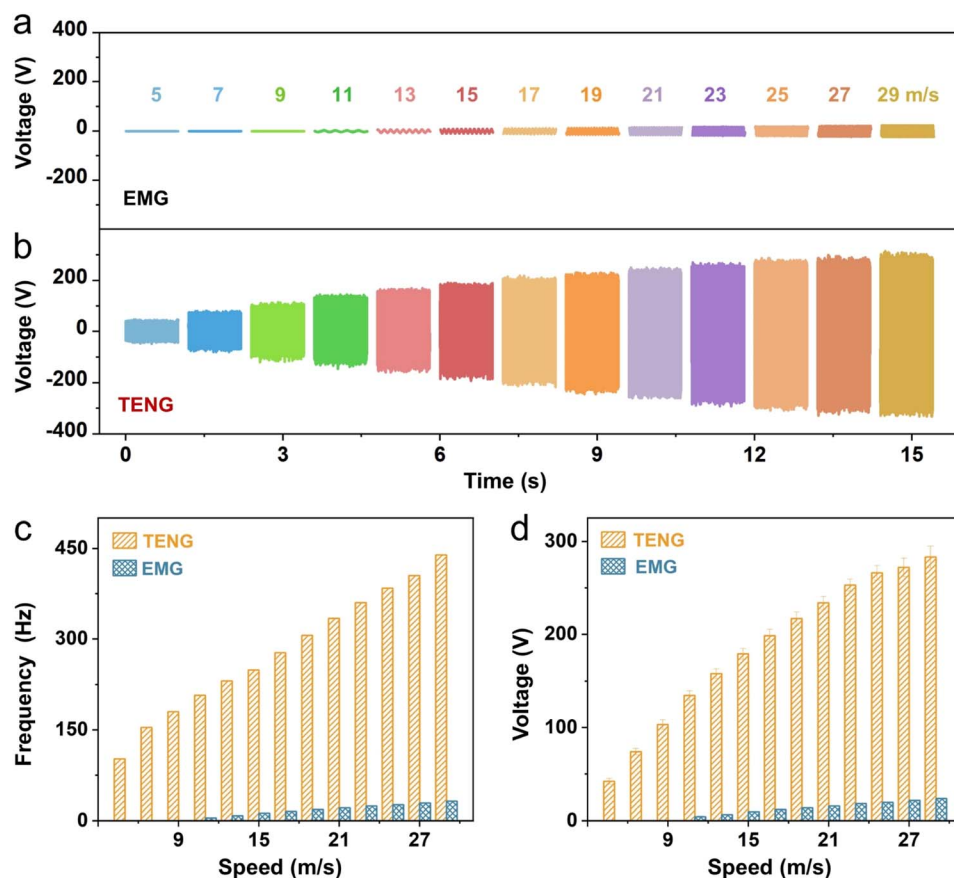

Fig. 2 Performance comparison of EMG and TENG at different wind speeds. (a) Output voltage of EMG at wind speeds of 5−29 m s^{-1}. (b) Output voltage of TENG at wind speeds of 5−29 m s^{-1}. (c) Comparison of output signal frequency of EMG and TENG at various wind speeds. (d) Comparison of average signal peak output voltage of EMG and TENG at various wind speeds.

This journal is © The Royal Society of Chemistry 2025

J. Mater. Chem. A, 2025, **13**, 9101–9110 | **9103**

compared to previously published wind harvesting TENGs, our TENG excels in withstanding higher speeds while achieving a high-frequency output, which provides possibilities for wind energy collection across a broader range of speed conditions.

2.2. Performance comparison of EMG and TENG at different speeds of the wind

In Fig. 2a, the load voltage produced by the EMG at speeds ranging from 5 to 29 m s^{-1} is illustrated, while Fig. 2b illustrates the voltage signals of the TENG at the same speeds as the wind. This indicates that the TENG can operate at lower speeds. Furthermore, the voltage signal generated by TENG is notably higher than that of the EMG. By increasing the voltage, the current on the transmission lines can be reduced, thereby decreasing line losses and making power transmission more efficient. We come across the following conclusions by extracting the voltages and frequencies in Fig. 2a and b for comparison. In Fig. 2c, we compare the frequency (f) of the electrical signals generated by both the TENG and EMG at different speeds. When the speed is 29 m s^{-1}, the frequency of the electrical signal generated by the EMG is 31.9 Hz. In contrast, the frequency of the output signal generated by the TENG is 439 Hz, approximately 13.7 times higher than the frequency of the EMG. This observation indicates that the frequency of the signal generated by EMG is much lower than that of TENG. The explanation lies in the benefits of the TENG structure we devised, where the vibrating layer is a thinner dielectric film, generating signals through the vibration of the dielectric film and friction with the electrodes. When the wind blows, the faster the frequency of the dielectric film's vibration, the higher the frequency of the generated signals. However, the EMG generates electricity by rotating around an axis, driving the rotation of the generator. The frequency of the generated signal is directly proportional to the rotational frequency. However, the rotational frequency of the EMG is much lower than the vibration frequency of the TENG's vibrating layer. Therefore, the TENG produces a higher signal frequency. In Fig. 2d, a significant difference is observed in the average output voltage signals of the EMG and TENG at various speeds. Notably, at a speed of 11 m s^{-1}, the voltage produced by the TENG is about 30.8 times higher than that of the EMG.

In general, the output power (P) of TENG is shown as the following equation:

$$P = \frac{U^2}{R} \tag{1}$$

where U represents voltage, and R is external total resistance, as shown as following equation:

$$R = \frac{R_0 \times r}{R_0 + r} \tag{2}$$

where r is the oscilloscope's internal resistance (in this case, $r = 10$ MΩ), R_0 is the external load resistor, and R is the resistance value after the parallel connection of r (oscilloscope) and R_0 (electrical load). Voltage measurements were conducted on both the EMG and TENG at varying speeds for different load resistances, facilitating the determination of output power at

various wind velocities, as shown in Fig. S2a and b.† The voltage curves corresponding to the maximum power point were then processed, and integration was performed to obtain energy as follows:

$$E = \int \frac{U^2}{R} \mathrm{d}t \tag{3}$$

where U symbolizes the voltage, R denotes the external total resistance, and t signifies time, which can be considered as representing energy (E). Fig. S2c and d† illustrate the wind energy (E) of both the EMG and TENG at different speeds respectively.

2.3. Performance and influencing factors of TENG operating at ultra-high speeds

It is deduced that the designed TENG's output performance may depend on factors such as the choice of material and thickness of the vibration layer, as well as the size of the TENG. Therefore, a range of conditions were examined to substantiate this hypothesis. To begin with, we experimented with different materials for the vibration layer of the TENG, which had an effective vibration size of 110 mm × 11 mm. We used various dielectric films, each with a thickness of 50 μm, such as polyamide66 (PA66), polyamide6 (PA6), polyimide (PI), fluorinated ethylene propylene (FEP), and polyethylene (PE). These films were selected to create friction and contact with the copper electrodes, generating triboelectric charge. The effective vibration size here indicates the area inside the double-ended fixed structure that may be involved in the contact separation mode for triboelectrification, which is different from the total size of the device. Subsequently, we evaluated the output voltage signals at varying speeds (ranging from 9 m s^{-1} to 81 m s^{-1}). Concurrently, additional conductive metal sheets, each with a thickness of 50 μm (comprising stainless steel, aluminum, and copper sheets), were employed to generate friction with a dielectric PA6 film. Subsequently, we measured their output voltage signals at different speeds, as shown in Fig. S4.† Fig. S3† demonstrates a schematic of the structure when the metal sheet interacts with the PA6 film through friction. Subsequently, for each speed, we compared the average peaks in the output voltage signal obtained from the friction between different dielectric films and copper electrodes (Fig. 3a). In addition, we compared the voltages generated by friction between the different metal sheets and PA6 film at varying speeds (Fig. 3b). Through our comparisons, we determined that when selecting a vibrating layer with the same thickness, metal sheets are more prone to damage and generally produce lower voltage signals compared to dielectric films. Further on comparing the dielectric films, when the vibration layer is a PI film, it is able to continue to generate a high voltage, even at 81 m s^{-1} speeds. In addition, compared with other evaluated materials, PI films exhibit excellent mechanical properties and friction resistance. Under the condition of ultra-high wind speed, the PI film is not easy to break or deform excessively, and can maintain good vibration stability. Based on these characteristics, we chose the PI film as the material of the vibration layer.

9104 | *J. Mater. Chem. A*, 2025, **13**, 9101–9110

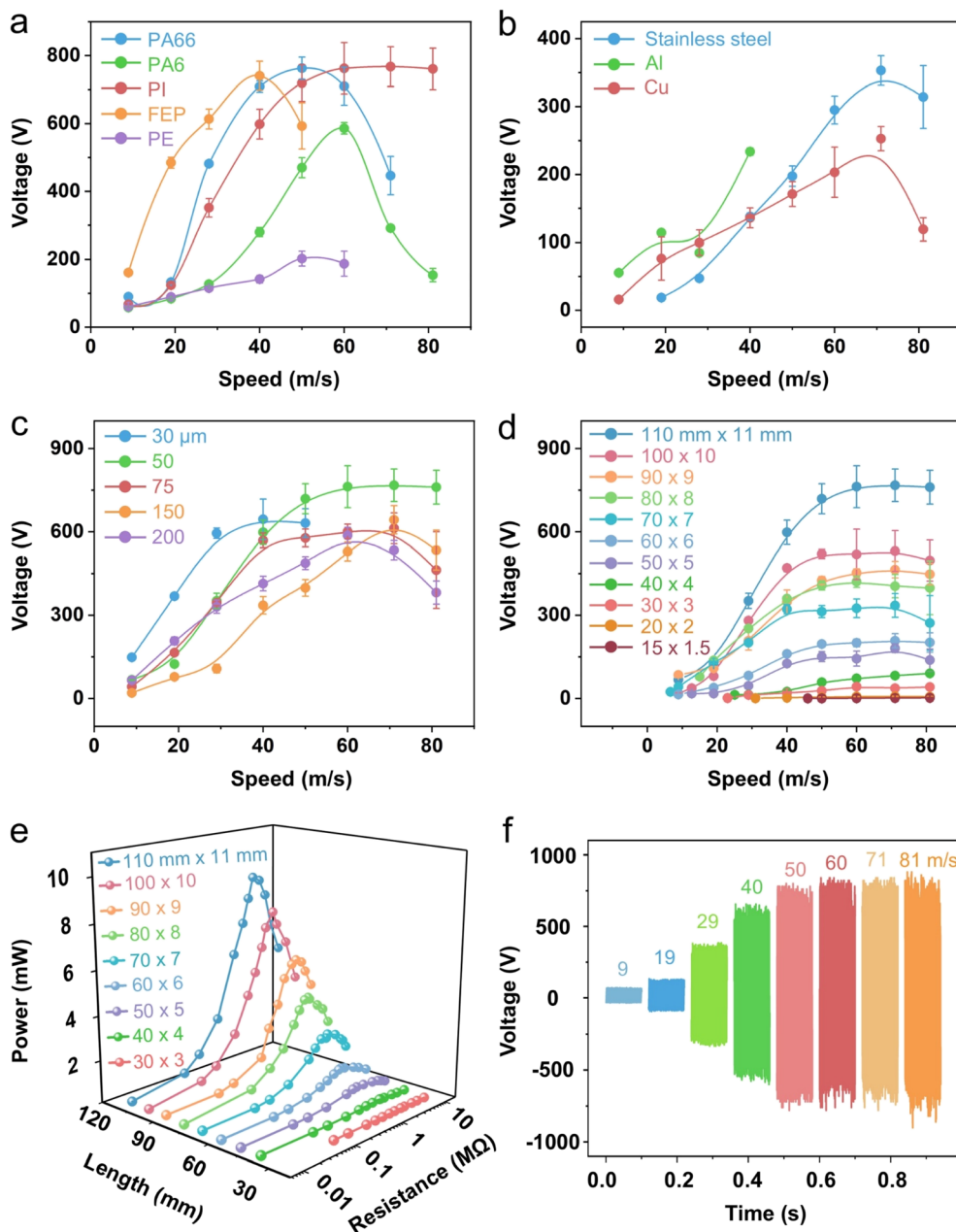This journal is © The Royal Society of Chemistry 2025

Fig. 3 Performance and influencing factors of TENG under high wind speeds. (a) Average voltage signal peaks of TENG with a dimension of 110 mm × 11 mm when the vibration layers are 50 μm dielectric films in frictional contact with Cu electrodes at different wind speeds. (b) Average voltage signal peaks of the TENG with a dimension of 110 mm × 11 mm when the vibration layers are 50 μm metal sheets in frictional contact with PA6 film at different wind speeds. (c) Average voltage signal peaks of TENG with dimensions of 110 mm × 11 mm at different vibration layer thicknesses at different wind speeds. (d and e) Average voltage signal peaks at different wind speeds (d) and output powers at 50 m s^{-1} wind speed (e) of the TENG with a 50 μm PI film vibration layer at different sizes. (f) Output voltage of the 110 mm × 11 mm TENG with a 50 μm PI film as vibration layer at different wind speeds.

With the friction material determined and optimized, the next step was to adjust the thickness of the vibration layer. For a TENG with an effective vibration size of 110 mm × 11 mm, we used PI films with thicknesses of 30, 50, 75, 150, and 200 μm, respectively, and evaluated their output voltages at different speeds (Fig. S5†). As shown in Fig. 3c, when comparing the average signal peaks of voltage values, we observed that using a very thin PI film resulted in the vibration layer breaking easily at high speeds. In contrast, if the vibration layer was too thick, it

led to suboptimal vibration and lower voltage generation. In addition, a thick vibration layer may pose challenges in initiating the system at low speeds. Therefore, we opted for a 50 μm thick PI film as the vibration layer since it produced a stable and relatively high voltage output. To investigate the performance of TENG further, we explored TENGs of different sizes, maintaining a fixed aspect ratio between their length and width.[30] We systematically investigated the output voltage signals of TENG devices of different sizes, ranging from an effective vibration

size of 15 mm × 1.5 mm to 110 mm × 11 mm, under varying speeds (Fig. S6†). By comparing the average output voltage signals of TENGs of different sizes, we observed that a larger sized TENG corresponds to larger frictional areas which result in higher output voltage signals (Fig. 3d). In addition, as shown in Fig. 3d, the cut-in wind speed increased as the device size was decreased. Furthermore, with increasing wind speed, the signal gradually increases; however, when the wind speed reaches a certain value, the signal tends to stabilize and no longer increases. In Fig. 3e, experiments were performed to determine

the output power (P) of TENGs with different dimensions. The device sizes were varied, spanning from an effective vibration dimension of 30 mm × 3 mm to 110 mm × 11 mm, under a constant wind speed of 50 m s^{-1}. Noticeably, the output power demonstrated an upward trend and was concurrent with the enlargement of dimensions of surface area; this can be related to the increased surface. Among them, the largest TENG has an output power of 8.9 mW. Finally, in Fig. 3f, we present the electrical signals of the TENG with an effective vibration size of 110 mm × 11 mm, using a 50 μm thick PI film as the vibration
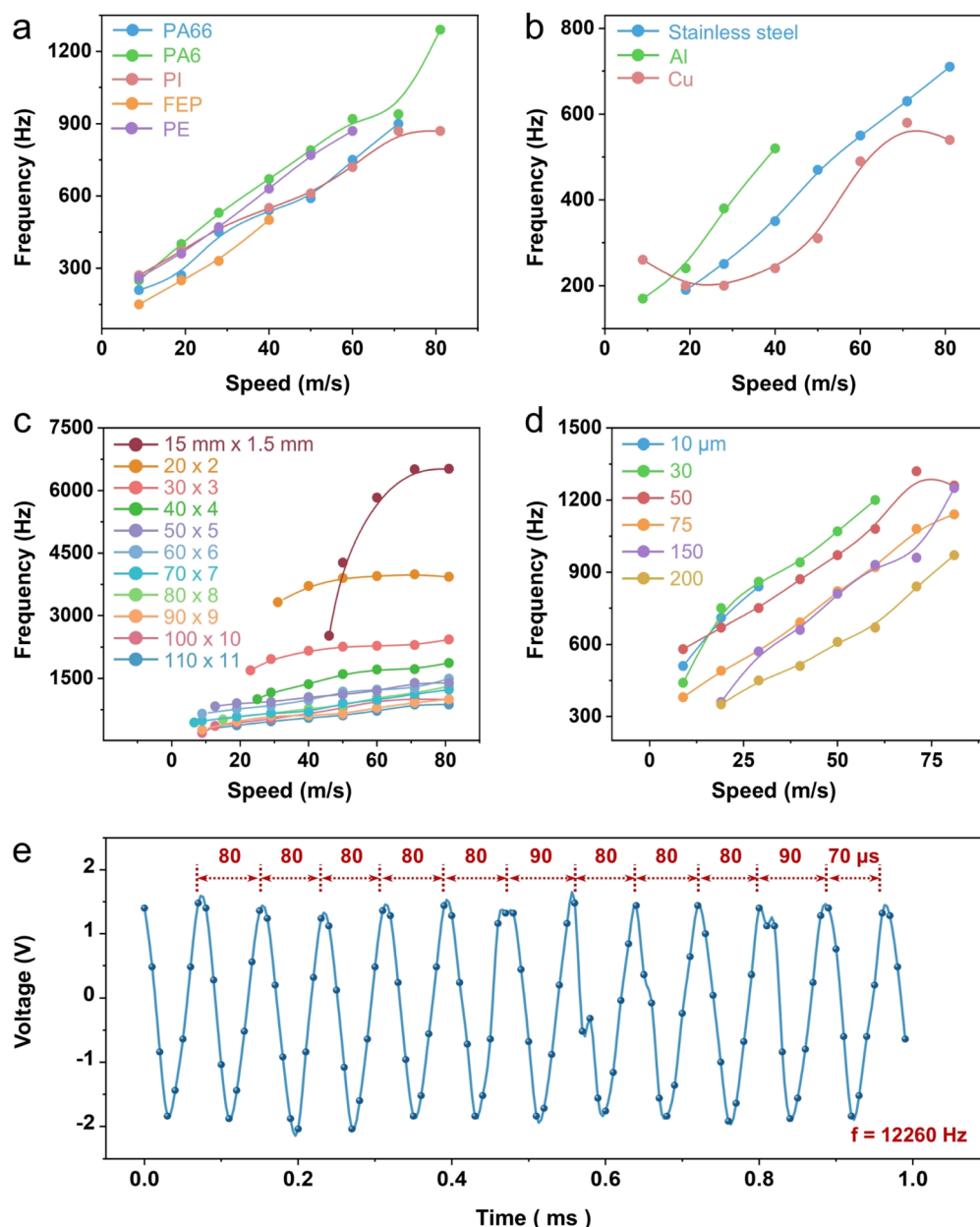

Fig. 4   Achieving high frequency signals in TENGs under ultra-high wind speeds. (a) Output single frequency of the TENG with a dimension of 110 mm × 11 mm when the vibration layers are 50 μm dielectric films in frictional contact with Cu electrodes at different wind speeds. (b) Output single frequency of the TENG with a dimension of 110 mm × 11 mm when the vibration layers are 50 μm metal sheets in frictional contact with PA6 film at different wind speeds. (c) Output single frequency of the TENG with a 50 μm PI film vibration layer with different sizes at different wind speeds. (d) Output single frequency of TENG with dimensions of 70 mm × 7 mm at different vibration layer thicknesses at different wind speeds. (e) Output single frequency of TENG with dimensions of 10 mm × 3 mm × 1 mm at 81 m s^{-1} wind speed.

9106 | J. Mater. Chem. A, 2025, 13, 9101–9110

This journal is © The Royal Society of Chemistry 2025

layer and friction with copper electrodes at different wind speeds. An experimental video can be found in Video S1,† which showcases the signal variations in the TENG as the wind speed rises, highlighting its sustained operation even at speeds surpassing 81 m s^{-1}. To protect the device and prevent the vibrating layer from breaking, we not only optimized the material, thickness, and size of the vibrating layer but also introduced a sponge as a damping layer. This design effectively alleviates the stress on the vibrating layer and reduces the risk of damage. Additionally, we designed the surrounding spacers of the vibrating layer as circular rings to further distribute the stress on the vibrating layer, thereby extending the service life of the TENG. Fig. S8b† illustrates the breakdown thresholds of the devices at various wind speeds.

2.4. Achieving high-frequency signals in TENGs at ultra-high wind speeds

High-frequency signal output is an effective way to reduce energy loss, while greatly improving energy conversion efficiency and increasing instantaneous energy density. With the continuous advancement of semiconductor technology and electronic circuits, the frequency of pulse power supplies will continue to increase, thereby achieving higher energy transfer efficiency and a wider range of applications. Fig. 4 illustrates the factors influencing the frequency of the output signal generated by the TENG devices. Fig. 4a and b show the frequencies of the signals generated by different materials when used as the vibration layer. This observation indicates that the signal frequency increases with an increase in wind speed, irrespective of the material used and whether or not they are conductive metal sheets or dielectric polymer films. Notably, the vibration frequencies of dielectric films are considerably higher than those exhibited by metal sheets. The influence of using different sizes of TENGs on the output signal frequency is significant; in Fig. 4c, a comparison is drawn among signal frequencies produced by devices for a range of sizes, spanning from an effective size of 15 mm × 1.5 mm to 110 mm × 11 mm, for different wind speeds. Fig. 4c reveals that a smaller device size consistently yields a higher signal frequency, and this trend becomes more pronounced as the device size decreases. When the effective vibration size is 15 mm × 1.5 mm, and the thickness of the vibration layer is 50 μm, the frequency generated is 6520 Hz at a wind speed of 81 m s^{-1}. It is interesting to note that the thickness of the vibration layer plays an important role in determining the frequency of the output signal of the device. Fig. S7† shows the voltage signals generated when a TENG with dimensions of 70 mm × 7 mm is evaluated using vibration layers with different thicknesses (10, 30, 50, 75, 150, and 200 μm) on being subjected to varying wind speeds. The reason for selecting a TENG of this size is that it enables the exploration of a broader range of vibrating layer thicknesses, thereby enhancing the scientific rigor of the experiment. Moreover, this size helps to reduce the damage of the vibration layer caused by ultra-high wind speed and ensure the stability and reliability of the experimental process. By calculating and comparing the frequency of voltage signals, it can be determined that a thinner vibration layer thickness results in higher vibration frequencies and, consequently, higher signal frequencies. However, thinner vibration films are more prone to breakage and failure at high wind speeds. Conversely, thicker vibration films yield significantly lower signal frequencies, as shown in Fig. 4d. After investigating and understanding the factors affecting output signal frequency, a TENG was constructed capable of high-frequency output by selecting small device dimensions and thinner vibration layers for our subsequent tests. We selected TENG devices with an effective vibration size of 10 mm × 3 mm, employing a 5 μm thick PI film as the vibration layer, and tested their voltage signals at a wind speed of 81 m s^{-1} (Fig. S8a†). Our analysis determined that the frequency of the output signal could reach 12 260 Hz, with a minimum time interval of only 70 μs between two peaks and the average time interval between two wave peaks is 80 μs, as shown in Fig. 4e. This highlights the TENG's capability to achieve a high frequency signal output. Here, we calculate the frequency of the signal it generates by analyzing the peaks of the signal data per unit of time. By increasing the frequency of the output signal, the current frequency becomes higher, causing the impedance to increase and thereby reducing the magnitude of the current. This effectively minimizes energy losses, leading to an improved energy output efficiency.

2.5. Performance and applications of larger-scale meter-dimension TENGs

In Fig. 5, we expand the dimensions of the TENG to evaluate its performance and applications in further detail. Fig. 5a showcases the progressively enlarged dimensions of the TENG, with the largest device achieving an effective vibration length of 1 m. In contrast to previous devices, we replaced the original acrylic substrate and copper foil electrode with a 5 mm thick aluminum alloy electrode plate, allowing the enlarged device to maintain its robustness and mechanical stiffness, while also achieving a high signal output. Subsequently, we employed an air blower to evaluate its output current and voltage signals when subjected to an average wind speed of 18 m s^{-1}, as shown in Fig. 5b and c. Due to the large outlet of the blower and uneven wind distribution, we selected twenty-one different positions laterally across the air blower and conducted ten wind speed measurements at each position. The attained average wind speed was 18 m s^{-1} and the fluctuation in average wind speed across distinct positions is delineated in Fig. S9a.† To emphasize the performance of the meter-sized device, we tested the output power and energy of devices with effective vibration sizes spanning 10 cm × 1 cm to 100 cm × 10 cm at a wind speed of 18 m s^{-1}. The highest output power reached 132 mW. In Fig. 5d and e, a comparison of the output power for different device sizes and the maximum output power and energy is presented. Consequently, we observed that the output power and energy increase with device size; however, when the device size reaches a certain threshold, the increase becomes less pronounced. This phenomenon may be attributed to charge loss in the friction layer due to increased size. In order to compare our device with the output signals of an electromagnetic generator at the
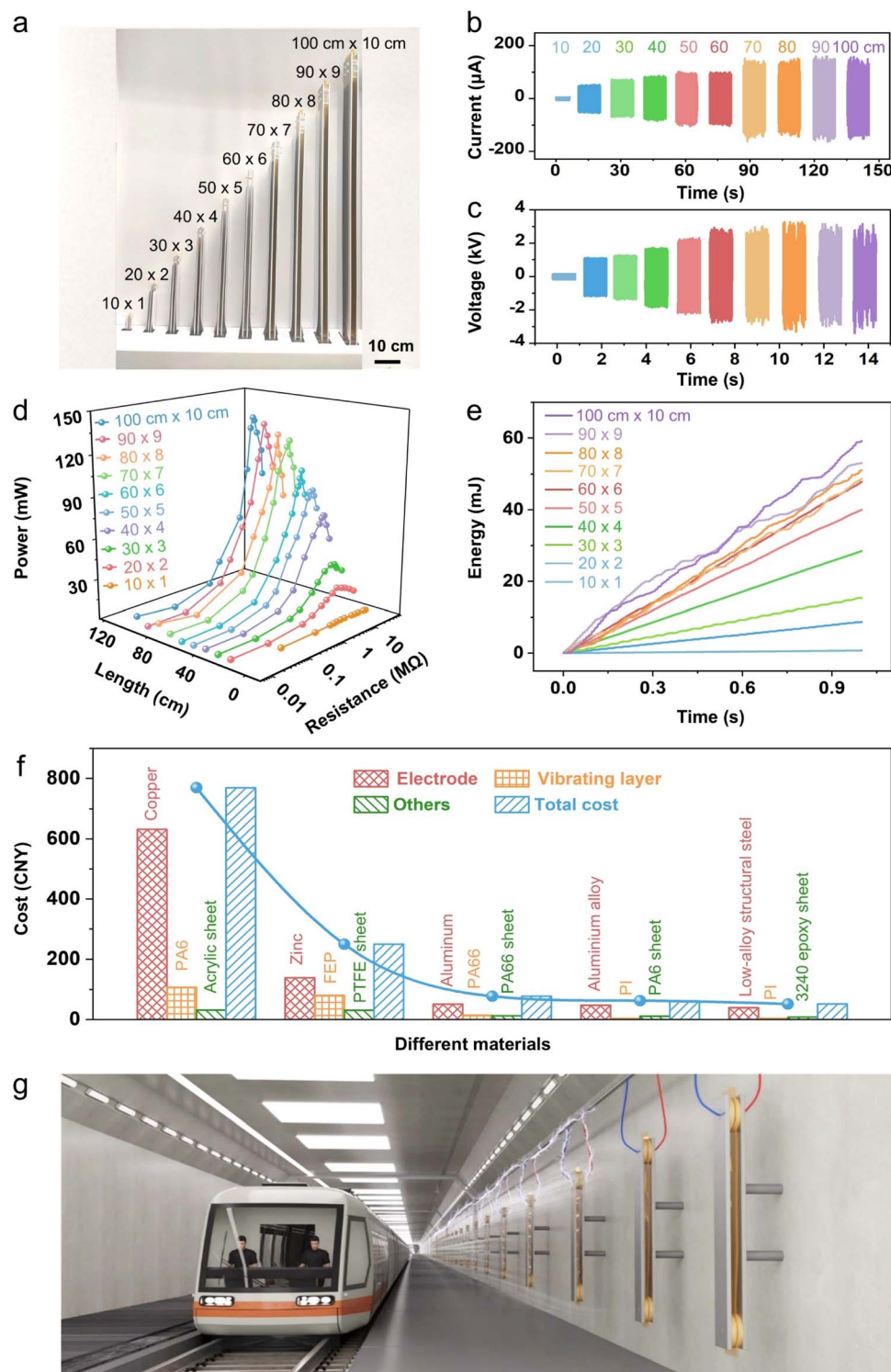
Fig. 5 Performance and applications of larger-scale meter-dimension TENGs. (a) Physical images of TENGs with different dimensions, up to 1 m in length. (b–e) Output current (b), voltage (c), power (d), and energy (e) of TENGs for a range of dimensions at an 18 m s^{-1} wind speed. (f) Price trends of different components for meter – sized TENGs. (g) Application prospects of integrated meter-sized TENGs in urban subway systems like powering subway speed warning systems.

same wind speed, we have presented the output current, output voltage, the relationship between voltage and output power, and the relationship between voltage and output energy of EMG at 18 m s^{-1} in Fig. S9b–e.†

In order to better integrate TENG and apply it to urban production, we reduce the unit cost of each component, such as the electrode, vibration layer, and padding material, to lower the overall device cost. Finally, it is possible to achieve a lower-

9108 | J. Mater. Chem. A, 2025, 13, 9101–9110

This journal is © The Royal Society of Chemistry 2025

cost device with an effective vibration length of 1 m. The cost variation with different materials is summarized in Fig. 5f. After reducing the device cost, it becomes feasible to mass-produce such devices in urban areas for harnessing wind energy. There are significant application prospects in various scenarios. For example, it is possible to install meter-sized TENGs next to subway tunnels within the subway system. When the subway passes through, it generates significant wind flow, causing the vibration layer of the device to oscillate and scavenge the wind energy for electricity generation. Devices not exposed to passing subways will remain inactive (Fig. 5g). The power generated by the TENG can be harnessed using electronic components like capacitors to collect and store energy. When integrated into an array, it can be used to supply power to underground speed alarm systems. Compared to conventional power supplies for these systems, the TENG offers advantages in terms of continuous and stable power generation while reducing energy waste.

3. Conclusion

Overall, this study advances the understanding of the potential of TENGs in wind energy harvesting under extreme wind conditions and provides insights into optimizing the TENG device design and performance. In this study, we have achieved the collection of mechanical wind energy at high speeds through a unique double-ended fixed structure TENG to simultaneously achieve a high and high-frequency signal output. Using this novel strategy, we have harvested wind energy at high speeds of 81 m s^{-1}, while maintaining lower manufacturing costs. Compared to an EMG, the TENG exhibits significant advantages in terms of voltage, frequency, applicable wind speed range, and cost. Compared to other TENG designs for harvesting wind energy, this work bridges the gap for harvesting wind energy at ultra-high speeds. The study investigated in detail the effects of materials employed, their sizes, and vibration layer thickness on the output voltage and frequency of TENG. When examining TENG devices of different sizes, when the device size is larger, the voltage signal is larger, however, the frequency of the generated signal will be reduced. As the thickness of the vibration layer is reduced, the frequency of the generated signal increases. Ultimately, by altering the length and thickness of the vibration material, we achieved a TENG with a frequency of up to 12 260 Hz. When we further increased the size of the TENG to meter-scale dimensions, it generated voltages exceeding 3000 V and the maximum output power was 132 mW. This paper therefore demonstrates that employing a double-ended fixed structure TENG provides a new and feasible strategy for collecting wind energy in more extreme weather and at ultra-high wind speeds and can be adapted to application scenarios in cities and urban environments.

4. Material and methods

4.1. Commercial source of EMG

An electromagnetic generator (Xiangsheng New Energy Technology, 5–20) was used to test the performance of conventional wind turbines.

4.2. Manufacturing of TENG

The wind-driven TENG structure was produced with a dual-sided fixed design. It incorporates a polyimide (PI) film as the friction layer and features two Cu electrodes. By employing a laser cutting machine (PLS4.75, Universal Laser Systems, USA), acrylic sheets measuring 138 mm × 11 mm × 3 mm were cut to serve as upper and lower support layers. Each of these layers was equipped with two 5 millimetre diameter holes at both ends. A 1 mm thick sponge was cut and attached to the acrylic sheets as a cushioning layer, and then the copper foil electrodes were connected to the sponge. The gap between the PI film and copper foil electrodes was 1.5 mm, and 5 mm holes were left at the corresponding positions for securing the sponge, PI film, and copper foil. Finally, bolts and screws were used to secure the holes, completing the operation of the double-ended fixed wind generator. In the end, we obtained a TENG with an effective vibration size of 110 mm × 11 mm × 3 mm.

4.3. Measurements

The TENG's output voltage was measured with a digital oscilloscope (MDO3024, Tektronix, USA), while the electrical signal from the TENG was analyzed using a computer-controlled Keithley 2611B. Influence by the oscilloscope's range and signal baseline, when testing devices with dimensions of 40 mm × 4 mm and larger, we used a probe with a load voltage of 40 MΩ. When the dimensions are below 40 mm × 4 mm, a probe with a load voltage of 10 MΩ is employed. When we measured commercial electromagnetic generators, we used a probe with a 10 MΩ load. High-speed wind tests were executed with a super high-speed motor (SMD-AT-500, ABB, Switzerland). To maintain an average wind speed of 18 m s^{-1}, a blower was employed to establish the necessary airflow conditions. The wind speed was measured using a differential pressure gauge (512, Testo, Germany).

Data availability

The data supporting this article have been included as part of the ESI.† More data can be provided upon request.

Conflicts of interest

There are no conflicts to declare.

Acknowledgements

References

1 B. O'Regan and M. Grätzel, *Nature*, 1991, **353**, 737–740.

This journal is © The Royal Society of Chemistry 2025

J. Mater. Chem. A, 2025, **13**, 9101–9110 | **9109**

2 A. V. Shah, H. Schade, M. Vanecek, J. Meier, E. Vallat-Sauvain, N. Wyrsch, U. Kroll, C. Droz and J. Bailat, *Prog. Photovoltaics*, 2004, **12**, 113–142.

3 Y. Yang, G. Zhu, H. Zhang, J. Chen, X. Zhong, Z.-H. Lin, Y. Su, P. Bai, X. Wen and Z. L. Wang, *ACS Nano*, 2013, **7**, 9461–9468.

4 R. Pelc and R. M. Fujita, *Mar. Policy*, 2002, **26**, 471–479.

5 L. He, C. Zhang, B. Zhang, O. Yang, W. Yuan, L. Zhou, Z. Zhao, Z. Wu, J. Wang and Z. L. Wang, *ACS Nano*, 2022, **16**, 6244–6254.

6 J. Wang, S. Zhou, Z. Zhang and D. V. Yurchenko, *Energy Convers. Manage.*, 2019, **181**, 645–652.

7 L. Zhang, B. Zhang, J. Chen, L. Jin, W. Deng, J. Tang, H. Zhang, H. Pan, M. Zhu, W. Yang and Z. L. Wang, *Adv. Mater.*, 2016, **28**, 1650–1656.

8 B. Chen, Y. Yang and Z. L. Wang, *Adv. Energy Mater.*, 2018, **8**, 1702649.

9 C. L. Archer and K. Caldeira, *Energies*, 2009, **2**, 307–319.

10 P. Veers, K. Dykes, E. Lantz, S. Barth, C. L. Bottasso, O. Carlson, A. Clifton, J. Green, P. Green, H. Holttinen, D. Laird, V. Lehtomäki, J. K. Lundquist, J. Manwell, M. Marquis, C. Meneveau, P. Moriarty, X. Munduate, M. Muskulus, J. Naughton, L. Pao, J. Paquette, J. Peinke, A. Robertson, J. Sanz Rodrigo, A. M. Semprevira, J. C. Smith, A. Tuohy and R. Wiser, *Science*, 2019, **366**, eaau2027.

11 S. Yong, J. Wang, L. Yang, H. Wang, H. Luo, R. Liao and Z. L. Wang, *Adv. Energy Mater.*, 2021, **11**, 2101194.

12 X. Chen, X. Ma, W. Ren, L. Gao, S. Lu, D. Tong, F. Wang, Y. Chen, Y. Huang, H. He, B. Tang, J. Zhang, X. Zhang, X. Mu and Y. Yang, *Cell Rep. Phys. Sci.*, 2020, **1**, 100207.

13 M. A. M. Hasan, W. Zhu, C. R. Bowen, Z. L. Wang and Y. Yang, *Nat. Rev. Electr. Eng.*, 2024, **1**, 453–465.

14 A. Ahmed, I. Hassan, M. Hedaya, T. Abo El-Yazid, J. Zu and Z. L. Wang, *Nano Energy*, 2017, **36**, 21–29.

15 X. Li, Q. Gao, Y. Cao, Y. Yang, S. Liu, Z. L. Wang and T. Cheng, *Appl. Energy*, 2022, **307**, 118311.

16 Y. Wang, X. Yu, M. Yin, J. Wang, Q. Gao, Y. Yu, T. Cheng and Z. L. Wang, *Nano Energy*, 2021, **82**, 105740.

17 Z. Quan, C. B. Han, T. Jiang and Z. L. Wang, *Adv. Energy Mater.*, 2016, **6**, 1501799.

18 C. Feng, S. Ji and W. Li, *Adv. Eng. Mater.*, 2024, **26**, 2400987.

19 H. Li, J. Wen, Z. Ou, E. Su, F. Xing, Y. Yang, Y. Sun, Z. L. Wang and B. Chen, *Adv. Funct. Mater.*, 2023, **33**, 2212207.

20 X. Fan, J. He, J. Mu, J. Qian, N. Zhang, C. Yang, X. Hou, W. Geng, X. Wang and X. Chou, *Nano Energy*, 2020, **68**, 104319.

21 H. Zhang, Y. Yang, X. Zhong, Y. Su, Y. Zhou, C. Hu and Z. L. Wang, *ACS Nano*, 2014, **8**, 680–689.

22 Y. Xie, S. Wang, L. Lin, Q. Jing, Z.-H. Lin, S. Niu, Z. Wu and Z. L. Wang, *ACS Nano*, 2013, **7**, 7119–7125.

23 S. Cho, Y. Shin, J. Choi, J. Eom, B. S. Oh, J. Lee and G. Y. Jung, *Nano Energy*, 2020, **77**, 105184.

24 W. Sun, Z. Ding, Z. Qin, F. Chu and Q. Han, *Nano Energy*, 2020, **70**, 104526.

25 J. Son, S.-H. Chung, K. Cha, S. Kim, Z.-H. Lin, J. Hong, J. Chung and S. Lee, *Adv. Mater.*, 2023, **35**, 2300283.

26 K. Fan, C. Chen, B. Zhang, X. Li, Z. Wang, T. Cheng and Z. Lin Wang, *Appl. Energy*, 2022, **328**, 120218.

27 W. Li, H. Guo, Y. Xi, C. Wang, M. S. Javed, X. Xia and C. Hu, *RSC Adv.*, 2017, **7**, 23208–23214.

28 X. Zhu, X. Cao and Z. L. Wang, *Adv. Mater. Technol.*, 2022, **7**, 2200006.

29 P. Wang, L. Pan, J. Wang, M. Xu, G. Dai, H. Zou, K. Dong and Z. L. Wang, *ACS Nano*, 2018, **12**, 9433–9440.

30 S. Wang, X. Mu, X. Wang, A. Y. Gu, Z. L. Wang and Y. Yang, *ACS Nano*, 2015, **9**, 9554–9563.

9110 | *J. Mater. Chem. A*, 2025, **13**, 9101–9110

This journal is © The Royal Society of Chemistry 2025